Lab-on-PCB 기술기반의 액체 단일추진제 마이크로 추진체 모듈의 연구 및 검증

Design, fabrication, and testing of a liquid monopropellant microthruster module using lab-on-PCB technology

초록

큐브위성 군집화에 있어 최적화된 추진체와 임무 종료 후 처리 장치의 부재는 실질적인 군집화 서비스 비즈니스 모델 개발에 걸림돌이 되고 있다. 본 연구는 Lab-on-PCB 기술을 활용한 나노위성용 마이크로 추진체 개발을 통해 이러한 도전과제를 해결하고자 한다. PCB에 플랫폼을 차용하여 촉매 점화 액체 단일 추진제 마이크로 추진체의 컨셉, 구성요소 설정, 및 조립 과정에 중점을 두었다. 본 마이크로 추진체는 수평 및 수직 유닛으로 구성된 추진체 모듈로 설계된 두 가지 유형의 50-mN 추진체로 구성된다. 개발된 PCB 추진체는 부피와 질량이 작고 지속적인 열 손실을 최소화한다. 표준화된 PCB 공정은 합리적인 비용에서 대량 생산을 가능하며, 상용화 및 확대 생산에 적합하다. 추진 시험을 통해 각 추진체 모듈의 분해 특성 및 효율성을 검증하고, Lab-on-PCB 기술이 추진체 모듈 제작에 적합한 해결책인지 확인한다. 또한, 추진체 모듈 레이아웃 보드을 통해 모듈 조립성을 극대화하였다. 본 연구는 Lab-on-PCB 기술의 우수성을 강조하며, 마이크로 추진체 개발에 대한 유망한 해결책으로서, 경쟁력 있는 나노위성 집단 구성 비즈니스 모델 개발의 단초가 될 것이다.

Key Words : Lab-on-PCB, hydrogen peroxide, monopropellant, microthruster, modular microfluidics

서 론

Satellite constellations have become increasingly versatile and commercially valuable, with applications ranging from building next-generation communication networks[1, 2] to observing the Earth and deep space[3-6]. However, the lack of suitable thrusters for nanosatellites, as well as a post-mission disposal device, poses a major obstacle to achieving the longevity and functionality required to develop a competitive nanosatellite constellation business model. Most commercial thrusters for nanosatellites have not been optimized; they require large mass and volume budgets for their implementation in satellites because the thruster market was focused on medium and large satellites until recently. Therefore, active research is being conducted on microthrusters to overcome this challenge[7-9] and adhere to the requirements of precise orbital and attitude control[10], sufficient lifespan through drag compensation, and post-mission disposal functions through deorbiting[11, 12].

Microthrusters for nanosatellites are primarily fabricated using micro-electromechanical systems (MEMS) and are subcategorized into electric and chemical propulsion thrusters[13]. Although electric propulsion produces a high specific impulse, it requires considerable power, which could significantly burden nanosatellites[14]. Conversely, chemical propulsion has high energy density and can generate a relatively large thrust with low power consumption, making it suitable for nanosatellites. Studies on chemical propulsion microthrusters have been extensively performed, with the majority focusing on traditional methods, such as using solid propellants[15, 16], bipropellants[17, 18], monopropellants[19-37], and cold gas[38, 39]. Solid-propellant microthrusters appeared in the early days and have been actively studied for their structural simplicity and suitability for miniaturization through packaging[15, 40, 41]. Despite these advantages, critical drawbacks have been identified: the thrust cannot be controlled, and additional algorithms and calculations are required for attitude control because the array type results in a thrusting pulse generated at a different location each time[33, 34]. However, despite their relatively simple structures, monopropellant thrusters can generate diverse long-term combustion and thrust profiles, which is impossible for solid-propellant microthrusters. In addition, the catalyst ignition method minimizes the probability of ignition failure during reignition, suggesting that monopropellant thrusters

are a suitable micropropulsion option for deorbiting and forming satellite constellations.

Silicon (125 W/m·K) was primarily used in early monopropellant microthruster applications, similar to other MEMS fields[20–23]. However, the high thermal conductivity of silicon and high volume-to-surface area ratio of its microstructure resulted in excessive thermal energy dissipation, causing low thermal efficiency. As a result, subsequent studies have attempted to construct microthruster hardware using various materials with low thermal conductivity. Several studies have reported that the microthrusters made with alumina[24], high-temperature co-fired ceramic (HTCC, 20 W/m·K)[25–27], and low-temperature co-fired ceramic (LTCC, 3.0 W/m·K)[29–31] showed improved thrust efficiency[28]. Some recent studies utilized glass, a high-insulation material (1.0 W/m·K)[32–36], with the results revealing the highest temperature efficiency (78%) among reported MEMS thrusters[36]. However, owing to the brittleness of glass, hardware components may become damaged by shocks or vibrations during transportation and launching. In addition, cracks may occur in the catalyst chamber because of the stress concentration caused by the thermal stress and internal pressure generated during the operation [34, 37]. In some cases, regenerative cooling channels are arranged above and below the combustor to relieve thermal stress[34]. Nevertheless, this process leads to lower efficiency owing to a decrease in the catalyst chamber temperature, which remains a challenge to be solved. Furthermore, the complicated production process, difficult standardization procedures, and limited material options of most existing microthrusters manufactured using MEMS make them unsuitable for upscaling and mass production[42, 43]; thus, several obstacles should still be overcome before commercialization.

These challenges are expected to be addressed using the lab-on-printed circuit board (PCB) concept, a rapidly emerging microfluidic technology. While it shares similarities with existing MEMS and lab-on-chip technologies, this concept is more centered on building a platform with integrated microfluidic and electronic control systems using PCB processes or products[44, 45]. FR-4 (glass-reinforced epoxy laminate material), with its satisfactory mechanical robustness and low thermal conductivity (0.2 W/m·K), is the most common material used in PCBs. In addition, the standardized PCB process enables mass production with precise dimensions at a reasonable cost, making it suitable for commercialization and upscaling[46, 48].

In this study, we experimentally investigated the concept of a 90 wt.% hydrogen-peroxide-based high-efficiency microthruster fabricated through the lab-on-PCB method. The concept, component configuration, and assembly process of a catalytically ignited monopropellant microthruster fully integrated into a PCB using the lab-on-PCB technology presented in this paper. The engineering model comprises two 50 mN thrusters designed as horizontal and vertical unit modules. The developed PCB thruster can be fabricated with a compact volume and weight, while the inherent material characteristics minimize heat loss, thus enabling robust operation; adopting a common commercial process guarantees economic effectiveness. The propulsion characteristics and efficiencies of each thruster module were verified through a series of propulsion experiments. Additionally, we present a substrate that facilitates an easy assembly of modules and an example application as a case study.

2. Architecture design

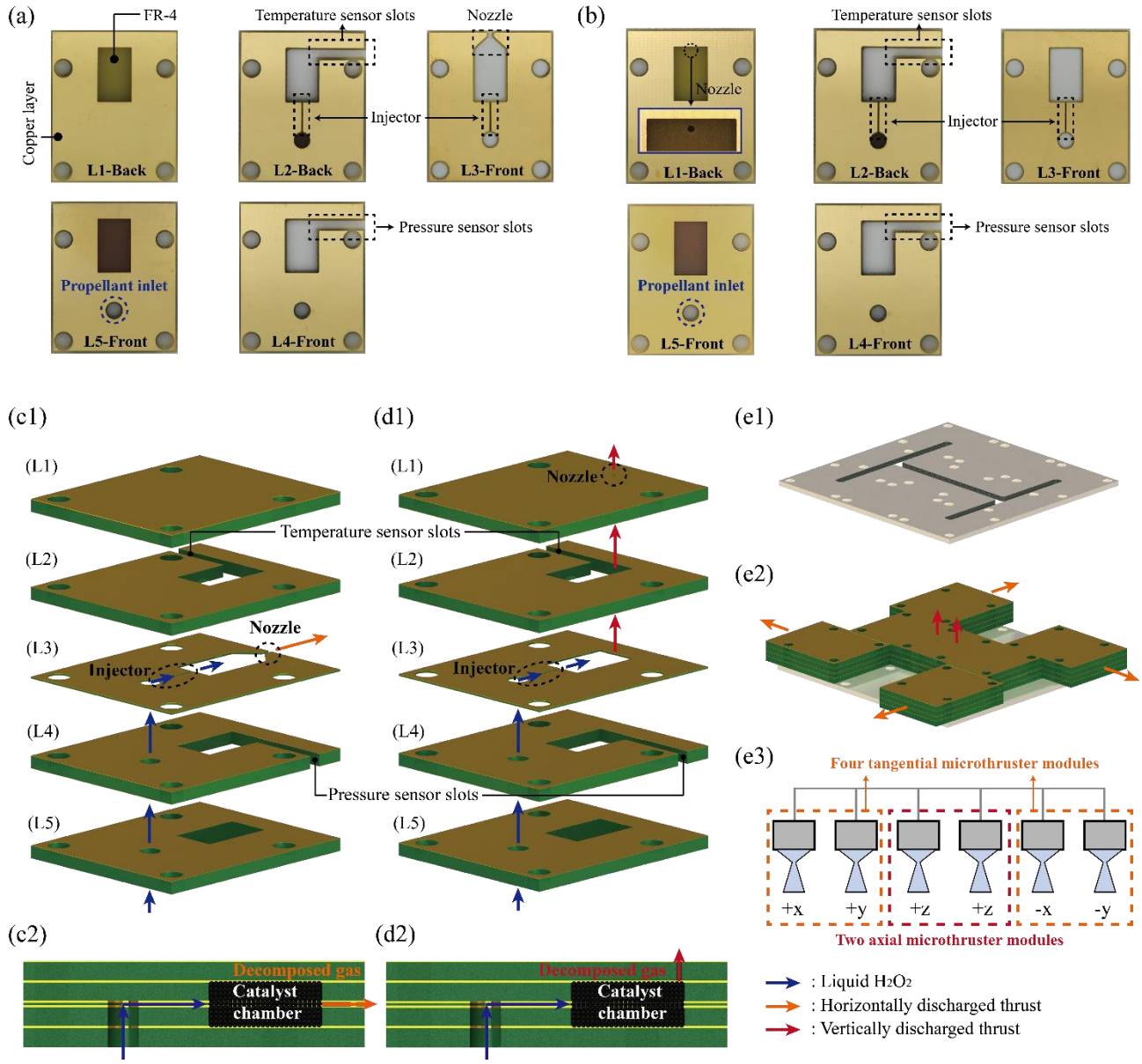

Fig. 1. (a) Five-layered PCB plates for fabricating a horizontal-type monopropellant microthruster, (b) PCB plates for fabricating a vertical-type thruster, (c1) detailed schematic of a horizontal-type thruster, (c2) operating process of the thruster from the propellant input (blue arrows) to the decomposed gas release (orange arrows), (d1) detailed schematic of the vertical-type thruster, (d2) operating process of the thruster from the propellant input (blue arrows) to the decomposed gas release (red arrows), (e1) thruster module layout board, (e2) one example of the modular thruster assembly, and (e3) schematic of the propulsion system.

The functional components of the microthruster were fabricated using a PCB manufacturing process and assembled using PCB surface mount technology (SMT). The horizontal/vertical thruster modules share the same design for the injector and catalyst chamber, with the only difference being the nozzle design. The glass-reinforced epoxy lamination material (FR-4), a common PCB board material, can be considered a subcategory of fiber-based ablative composites[49–51] and exhibits a high ablation resistance[52]; therefore, it minimizes performance degradation owing to structural deformation and provides long-term stability. The PCB plates used to assemble each type of thruster, as shown in Fig.

1(a) and 1(b), were fabricated by a PCB manufacturer (Hansaem Digitec, South Korea). Each thruster consisted of five 25 × 30 mm plates labeled L1–L5 (hereafter referred to as Plate L1–L5). Plate L3 was composed of a 0.25-mm-thick FR-4 substrate, whereas the remaining four plates were made of 1.6-mm-thick FR-4 substrates. All plates had a 35-μm-thick copper layer on their upper and lower surfaces to enable plate assembly through the soldering process, a PCB SMT method. Each plate featured four holes with diameters of 3 mm, which enabled mounting on the board after aligning and assembling the thruster module using M3 bolts. Plate L5 housed a monopropellant inlet, and the injector's lower and upper halves were patterned on the back surface of Plate L2 and front surface of Plate L3, respectively. Furthermore, a rectangular hole was processed through Plates L2 to L4, creating a catalyst chamber that mounted the granule-type MnO_2/Al_2O_3 catalyst. For temperature and pressure measurements, 1.6-mm-wide sensor slots were processed on the sides of Plates L2 and L4. A horizontal thruster nozzle was fabricated in L3, and a vertical thruster nozzle was fabricated in L1. Notably, all the fabrication processes were performed using a precise yet cost-effective standardized PCB fabrication method.

The operating principle of the thruster is illustrated in Fig. 1(c) and 1(d). The monopropellant was first input into the L5 inlet using a syringe pump, after which it flowed into the catalyst bed through the patterned injector on Layers L2 and L3. Inside the chamber, the MnO_2/Al_2O_3 catalyst decomposed the monopropellant, generating gas that accelerated through the nozzle and produced thrust.

The two types of thrusters capable of generating unit thrust can be conveniently combined in various configurations on a 10 × 10 cm PCB-based thruster module layout board (Fig. 1(e1)). This layout board can be attached to both the thruster module and satellite body through a 3-mm-diameter hole, functioning similarly to an optical table. The horizontal/vertical thruster module can be configured to enable thrust generation along the ±x, ±y, and +z axes, as illustrated in Fig. 1(e2) and 1(e3), for utilization in satellite missions. By varying the thruster types, quantities, and arrangements, it was possible to create propulsion systems with diverse performance capabilities beyond the suggested combinations.

3. Materials

3.1. Propellant selection

Monopropellants are used to generate thrust from high-energy gases via catalytic decomposition or combustion. Although hydrazine has traditionally been the primary monopropellant used in commercial thrusters, concerns regarding its toxicity and environmental impact have sparked interest in eco-friendly alternatives. Green monopropellants offer a higher density-specific impulse than conventional propellants, which is advantageous for reducing the size of propellant tanks. Notable green monopropellants include hydrogen peroxide (H_2O_2), HAN (NH_3OHNO_3), and ADN ($NH_4N(NO_2)_3$)[53]. In this study, hydrogen peroxide was selected as the monopropellant owing to its nontoxic nature, cost-effectiveness in terms of safety facility requirements during thruster development and testing, and ability to decompose without preheating. However, its relatively low specific impulse is a drawback. Ongoing research is actively exploring the incorporation of hydrocarbon fuels to overcome this limitation[54–57]. Therefore, the development of hydrogen peroxide-based lab-on-PCB thrusters has the potential for broad scalability in monopropellant utilization. During the decomposition of hydrogen peroxide, steam and oxygen are produced, generating a heat energy of 2884.47 kJ/kg at a concentration of 100 wt.%. In this study, a monopropellant composition of 90 wt.% hydrogen peroxide with a density of 1.392 g/cm³, was utilized, and the measured adiabatic decomposition temperature was 1022 K.

3.2. Catalyst preparation

To address the rapid heat dissipation in microthrusters, MnO_2/Al_2O_3 granules were used as a catalyst to enhance the propellant decomposition efficiency. Many previous studies have formed a structure inside the chamber and coated the inner surface with an active material; however, they often encountered limitations in achieving sufficient decomposition efficiency and durability. This can be

achieved by coating granule-type porous catalyst supporters with sufficient mechanical properties, heat resistance, and chemical stability. γ-Al_2O_3 was selected as the catalyst supporter material owing to its high specific surface area (234.81 m^2/g), strong adhesion to metals, and resistance to surface area decrease at a hydrogen peroxide decomposition temperature[58, 59]. Manganese, widely used as a monopropellant decomposition catalyst, was selected as the active material to be loaded onto the supporter and fabricated using a method suggested in previous studies[60, 61].

In the catalyst fabrication process, 1/8-inch γ-Al_2O_3 pellets were pulverized and filtered through a sieve with a mesh size of 35-40. Particles with diameters ranging from 425 μm to 500 μm were carefully selected and subjected to thorough washing. The size of the support was determined to be 1/10 the chamber diameter, considering the propellant residence time and pressure drop. To impregnate Mn onto the γ-Al_2O_3 granules, a 40 wt.% aqueous solution of $NaMnO_4$ (Dongmoon Chemical Co., South Korea) was used as the precursor. We intended to dope 27.8 wt.% Mn to fabricate the MnO_2/Al_2O_3 catalyst; therefore, 32.65 g of the precursor solution was poured into a 75-mm-diameter beaker, ensuring that the γ-Al_2O_3 granules were completely immersed, and the solution was stirred until the granules were completely wet. The beaker was then dried in a convection oven at 120 ℃ for 22 h. Subsequently, the dried catalyst was transferred to an alumina crucible and calcined in an electric furnace at 500 ℃ for 5 h. Finally, after washing the resulting catalyst, it underwent further drying in a convection oven at 120 ℃ for 22 h to complete the fabrication process.

Fig. 2. Fabricated MnO2/Al2O3 catalyst with a support mesh size of 35-40, 425-500 μm

Figure 2 shows a photograph of the fabricated catalyst granules. Following catalyst production, two key analyses were performed[62]: measurement of the specific surface area and determination of the amount of doped Mn. The specific surface areas of the catalysts were measured three times using the Brunauer-Emmett-Teller (BET) method with a Tristar II 3020 instrument (Micromeritics, USA). Nitrogen adsorption was performed at 73 K during the measurements. The average surface area was 70.63 m^2/g. Additionally, the amount of Mn doped onto the MnO2/Al2O3 catalyst was quantified using inductively coupled plasma optical emission spectrometry (ICP-OES) with an iCAP6300 instrument (Thermo Fisher Scientific Co., USA). Before the analysis, 50 mg of the MnO_2/Al_2O_3 catalyst was pretreated with 5 mL of aqua regia and 0.5 mL of sulfuric acid and heated at 170 ℃ for 30 min to dissolve the catalyst. The resulting mixture was diluted with a known volume of water, and the Mn concentration was measured. The doping concentration of Mn was 26.0 wt%, which closely approximates the desired value of 27.8 wt%.

4. Design and fabrication of PCB microthruster modules

4.1. Microthruster design

In this study, considering the thrust range of nano-and microsatellites, we carefully selected 50 mN

as the target thrust of the microthruster and verified the feasibility of the PCB fabrication for microscale thruster components. Using the chemical equilibrium with applications (NASA CEA), the estimated specific impulse and characteristic velocity of the microthruster are 87.8 s and 936 m/s, respectively, under a thruster chamber pressure of 3 bar and nozzle exit pressure of 1 atm.

$$F = \dot{m} I_{sp} g_0 \quad (1)$$

$$P_c = \dot{m} C^* / A_t \quad (2)$$

The mass and volume flow rates of the propellant were 3.486 g/min and 2.50 mL/min, respectively, calculated using the thrust equation, Eq. (1). Using the calculated factors, the main components of the microthruster—catalyst chamber, injector, and nozzle—were designed. The detailed dimensions and shapes of the horizontal and vertical thruster modules are shown in Fig. 3 and are listed in Table 1. In addition, the horizontal and vertical thrusters were designed to have the same dimensions as the remaining components, except the nozzle.

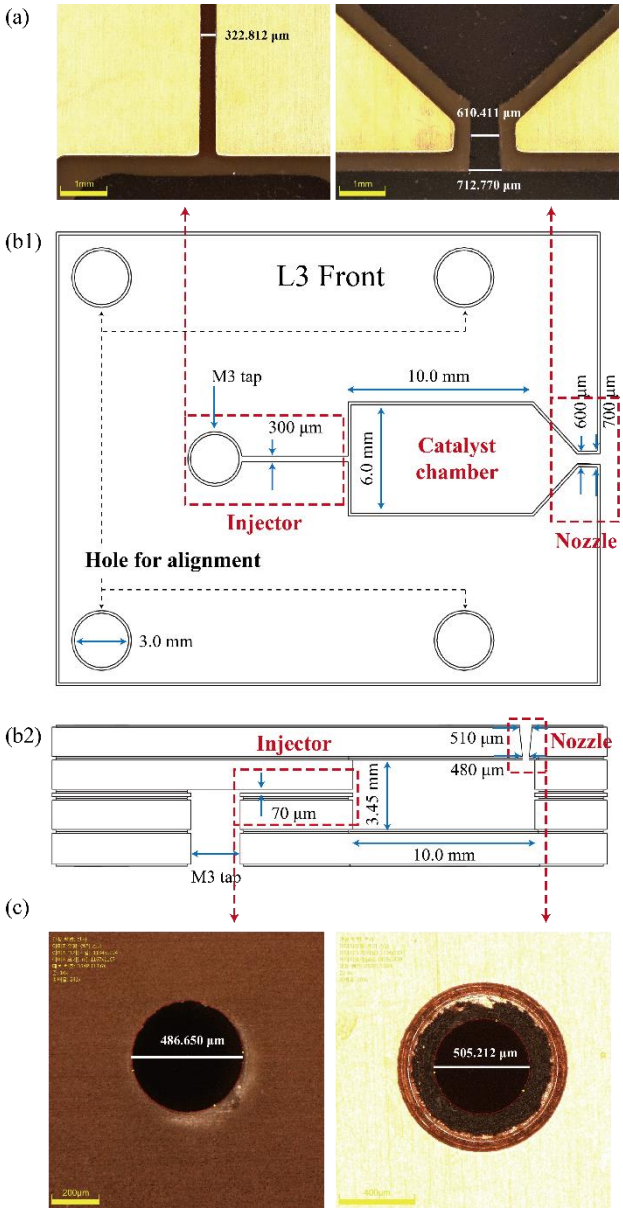

Fig. 3. (a) Image of measured dimensions of the injector and nozzle of the horizontal thruster. (b) Dimensions of the designed thruster: (b1) Main component dimensions of the horizontal- and (b2)

vertical-type thrusters. (c) Images of measured diameters of nozzle throat and exit of vertical thruster.

Table 1. Specifications of the designed PCB microthruster

Properties	Value
Thrust	50 mN
Chamber pressure	3.0 bar
Specific impulse at sea level	87.8 s
Characteristic velocity	936 m/s
Propellant mass flow rate	3.486 g/min
Injector pressure drop	0.43 bar
Catalyst capacity	0.50 (g/s)/cm^3
Catalyst chamber dimension (L×W×H)	10×6×3.52 mm
Nozzle throat area	0.18 mm^2
Expansion ratio of nozzle	1.13

Injector: The pressure drop at the injector was set to 5–20% of the chamber pressure to dampen the catalyst chamber pressure instability[63]. The injector dimensions were set to generate a pressure drop of 14.3%. The injector was patterned on a 35-micrometer-thick copper layer at the back of Plate L2 and in front of Plate L3 with dimensions of 300 μm width and 7.5 mm length. The actual machined dimensions were 322.812 μm, which resulted in a machining error of 7.60%, and this could cause a slightly lower pressure drop than the expected designed value.

Catalyst chamber: To determine the dimensions of the catalyst chamber, the mass flow rate of hydrogen peroxide and catalyst capacity of Mn were required. In previous microthruster research, platinum was used as a catalyst, with a catalyst capacity of 0.6~1.03 (g/s)/cm^3[33, 34, 63] to design a thruster. We used a conservatively determined catalyst capacity of 0.5 (g/s)/cm^3, considering the relatively large granule size. The volume of the catalyst chamber was considered by its definition; the mass flow rate of decomposable hydrogen peroxide per unit volume of catalyst. Therefore, the fabricated dimensions of the chamber were 6.0 mm width, 10.0 mm length, and 3.52 mm depth for sufficient propellant decomposition.

Nozzle: Under a chamber pressure of 3 bar, the exhaust Mach number of the nozzle was calculated as 1.402, with an expansion ratio of 1.13. The nozzle throat area of 0.18 mm^2 was calculated using Eq. (2), while the nozzle exit area was 0.203 mm^2. The nozzle of the horizontal-type thruster, which included copper layers, was made of Plate L3 with a total thickness of 320 μm; the dimensions of the nozzle throat and exit were designed to be 600 μm and 700 μm, respectively. The fabricated nozzle dimensions were 610.411 μm and 712.770 μm, and the processed with an error of 1.74% and 1.82%, respectively. The vertical nozzle was processed on Plate L5 with a thickness of 1.6 mm, where the dimensions of the nozzle throat and exit were 480 μm and 510 μm, respectively, and the fabricated nozzle dimensions were 486.650 μm and 505.212 μm, with an accuracy of 1.39% and 0.94%, respectively.

4.2. Assembly process

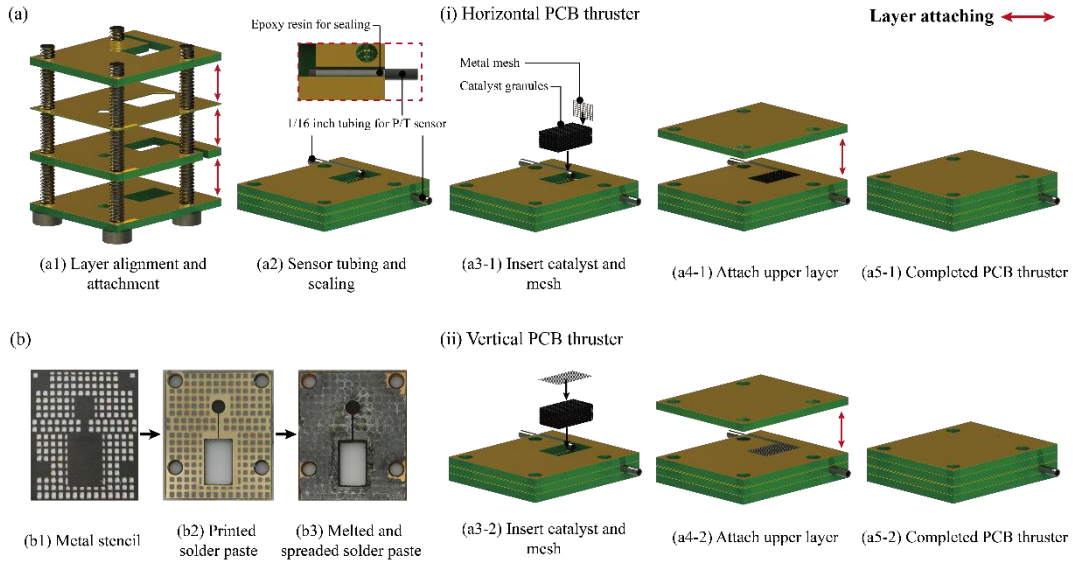

Fig. 4. (a) Integration process for fabricating a microthruster. (b) Layer attachment process using the PCB SMT method.

Figure 4(b) illustrates the layer attachment process of the PCB plate. The process involves the application of an epoxy solder paste (RSFP240-T4, Hojeonable Inc., Korea) onto the copper layer of the PCB through stencil printing, followed by soldering. The detailed process is as follows. First, a metal mask with a thickness of 0.1 mm was prepared in the form of a mesh with 1 × 1 mm square holes separated by a distance of 0.6 mm to apply an appropriate amount of paste (Fig. 4(b1)). The metal mask and PCB block were then aligned, and an epoxy-solder paste was printed on the copper layer of the PCB with a squeeze blade. The paste was patterned onto the copper layer after the metal mask was removed (Fig. 4(b2)). Subsequently, the epoxy-solder paste was melted in a reflow oven, spread over the copper layer, and cured to perform face-to-face attachment (Fig. 4(b3)). The process involved heating at a rate of 1.5 ℃/s, melting at 249 ℃ for 7.5 min, and then cooling at a rate of 1.5 ℃/s.

Figure 4(a) illustrates the assembly process of the PCB thruster. The horizontal- and vertical-type thrusters were assembled in the same order except for the stainless steel (SUS) mesh arrangement. The paste was applied to Plates L5 to L2, and they were stacked by being aligned with M3 bolts (Fig. 4(a1)). Subsequently, a 1/16-inch-diameter pipe and thermocouple were inserted into the sensor slots of Plates L2 and L4, respectively, and sealed with quick-curing epoxy (Fig. 4(a2)). During this process, the upper surface of Plate L2 was masked with Kapton tape to avoid the epoxy coming on the copper layer. The catalyst chamber was filled with MnO_2/Al_2O_3 granules after the mask was removed (Fig. 4(a3)). To prevent granule escape, the SUS mesh can sufficiently screen the nozzles of horizontal- and vertical-type thrusters. Finally, the epoxy-solder paste was applied to the bottom of the Plate L1 plate and combined with Plates L5 to L2 specimens (Fig. 4(a4)) to complete the thruster (Fig. 4(a5)).

5. Results of propulsion experiments

5.1. Experimental setup

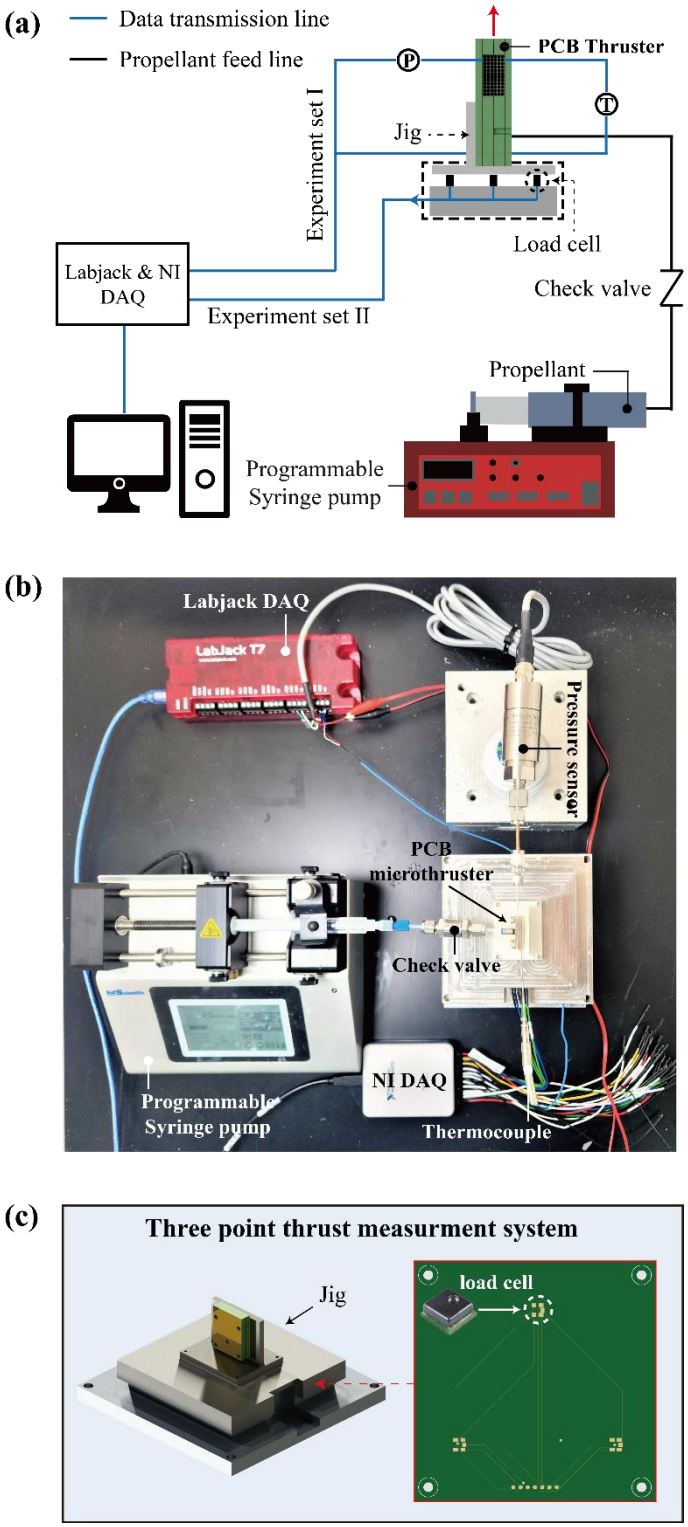

Fig. 5. (a) Experimental setup for monopropellant supply and thrust measurements. (b) Photograph of the equipment setup for performance testing. (c) Three-point thrust-measurement device.

Several propulsion tests were conducted to verify the propulsion characteristics and efficiencies of the two types of PCB monopropellant microthruster modules. A schematic of the system for propellant supply and propellant characteristic evaluation is shown in Fig. 5. A syringe pump (KDS 210, KD

Scientific Co. Ltd, USA) and 3.0 mL of a gas-tight Luer lock-type syringe were used as propellant suppliers. An outer diameter of a 1/16-inch Teflon tube was used for piping the propellant transfer, considering its compatibility with hydrogen peroxide and the time it resided in the pipe. A check valve was used to prevent abnormal pressure behavior and countercurrents caused by pipe blockage. The pressure, temperature, and thrust were measured to evaluate the thrust characteristics. Owing to the small amount of generated thrust, simultaneously obtaining precise thrust and temperature/pressure measurements may prove difficult because of the mechanical resistance of multiple sensing pipe fittings. Therefore, pressure, temperature (Section 5.2), and thrust (Section 5.3) of the horizontal- and vertical-type thrusters were separately measured for different sets of experiments.

Figure 5(b) shows a photograph of the experimental setup used for the measurements. The chamber pressure of the microthruster was measured using a pressure transducer (PSHB0010BGPG, Sensor System Technology Co. Ltd., South Korea) connected to the sensor slot of the thruster with a stainless-steel tube. The pressure sensor had a measurement range of 0 to 10 bar and an accuracy of ±0.15%FS. The temperature was measured using a K-type thermocouple with the 1/16-inch probe capable of measuring temperatures ranging from −200 °C to 1350 °C. Thrust was measured using a microthrust measuring system equipped with a load cell. Figure 5(c) shows the configuration of the three-point thrust measurement system, consisting of a rigid plate with a jig that holds the microthruster placed on ball-type load cells (FMAMSDXX005WCSC3, Honeywell, USA) arranged in an equilateral triangle pattern. The measurement range of each load cell was 0–5 N, and the resolution was approximately 0.3 mN. Generated thrust was measured by acquiring three reaction force data from each load cell and adding them together. Temperature and pressure data were collected using a data acquisition device, DAQ (T7, Labjack, USA), and thrust data were collected using a DAQ (NI USB-8452, National Instruments, USA).

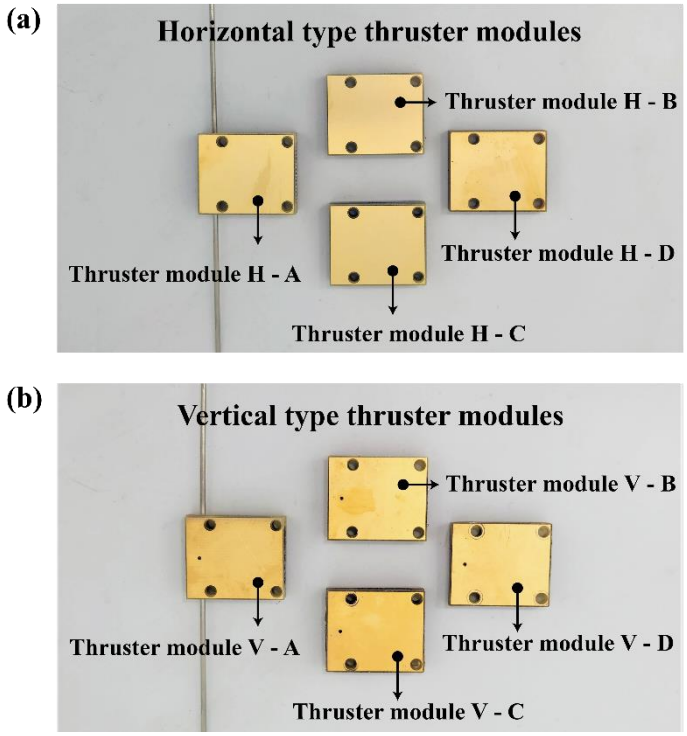

Fig. 6. Photos of the thruster modules for performance and repeatability verification. (a) Horizontal-type thruster module: H – A, B, C, and D, (b) Vertical-type thruster module: V – A, B, C, and D.

Figure 6 shows a photograph of the thruster utilized in each experimental set, where Fig. 6(a) shows horizontal-type thruster modules and Fig. 6(b) shows vertical-type thruster modules. The test was performed as follows: To verify the repeatable and reliable performance of the PCB microthruster modules, a pulse-mode firing test was conducted. Before the main experiment set, the propellant was

injected into the microthruster module twice for 5 s at 10% of the main mass flow rate for the hot-start mode. Each cycle of the main propulsion test consisted of a propellant supply phase lasting for 10 s, followed by a rest phase of 10 s. The repeatability of the modules was assessed by executing three cycles using the same pattern. Thruster modules H – A and V – A were fabricated for pressure and temperature measurements, and three thrusters of each type (thruster modules H – B, C, D, and Thruster modules V – B, C, and D) were employed for thrust measurements to validate the repeatability of the system.

5.2. Performance test results: Pressure and Temperature

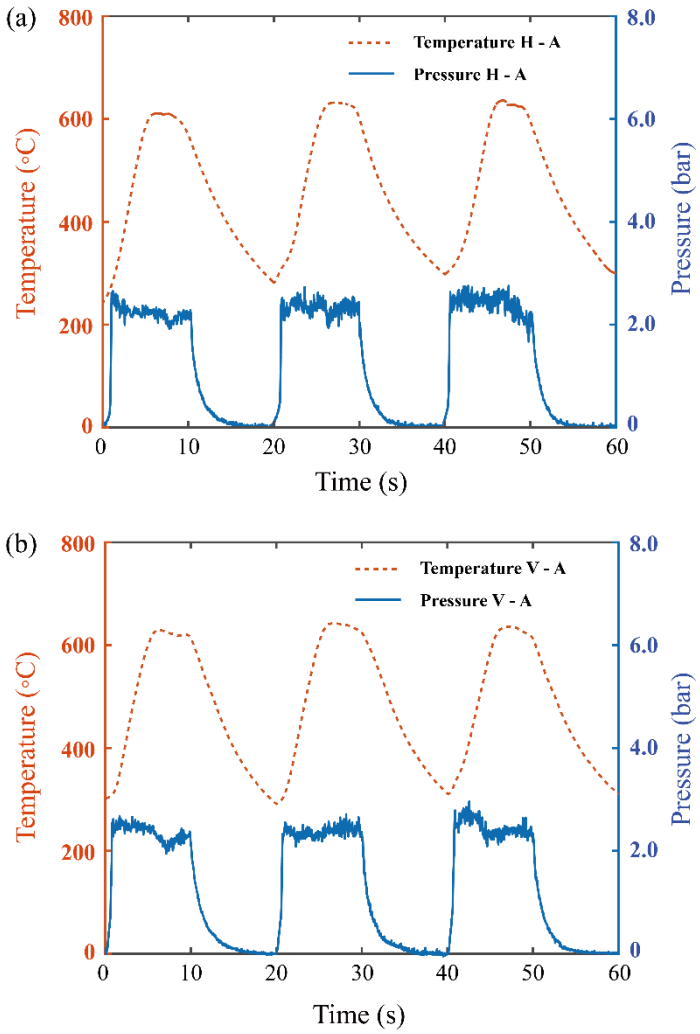

Fig. 7. Chamber pressure and temperature measurement results from a pulse-mode firing test: (a) Horizontal thruster module A and (b) vertical thruster module A.

Table 2. Experimental results of pressure and temperature thruster modules.

	Cycle I	Cycle II	Cycle III	Avg.
Temp. H-A	611.21 ℃	631.99 ℃	636.33 ℃	626.51 ℃
Pressure H-A	2.218 bar	2.302 bar	2.374 bar	2.298 bar
Temp. V-A	629.99 ℃	642.65 ℃	636.01 ℃	636.22 ℃
Pressure V-A	2.317 bar	2.333 bar	2.411 bar	2.354 bar

Figure 7 shows the results of three cycles of the pulse-mode firing tests of the horizontal and vertical thruster modules. Table 2 lists the peak and steady-state pressures for each cycle. The maximum peak temperatures of the horizontal and vertical thruster modules were 636.33 ℃ and 642.65 ℃, respectively. In addition, the measured average steady-state chamber pressures were 2.298 and 2.354 bar for the horizontal and vertical thruster modules, respectively. Based on the results of the performance tests, the horizontal and vertical thruster modules exhibited similar decomposition temperatures and chamber pressures. However, the slight differences observed can be attributed to variations in the nozzle throat area. The designed nozzle throat area was intended to be 0.18 mm^2, but owing to processing errors, the actual measured horizontal and vertical nozzle throat areas were 0.195 mm^2 and 0.186 mm^2, respectively. These differences can be minimized by fabricating more accurate dimensions considering the errors that occur during the process.

$$\eta_{\mathrm{Temp}} = (T_{\mathrm{c,exp}} - T_{\mathrm{room}})/(T_{\mathrm{c,theo}} - T_{\mathrm{room}}) \quad (3)$$

$$\eta_{\mathrm{C^*}} = {C^*}_{\mathrm{exp}}/{C^*}_{\mathrm{theo}} \quad (4)$$

The temperature and C* efficiency were calculated using Eq. (3) and (4), respectively: These calculations enable a quantitative evaluation of the thruster performance. The temperature efficiency, ηtemp, was determined by considering an upper limit of 749 °C for the decomposition temperature of 90 wt% hydrogen peroxide and a lower limit of 25 °C for room temperature. Calculations were performed to evaluate temperature efficiency at the maximum peak temperature. For the horizontal and vertical thruster modules, the temperature efficiencies were 84.44% and 85.31%, respectively. Previously conducted studies on MEMS-based microthrusters utilizing 90 wt% hydrogen peroxide as a propellant reported experimentally measured maximum values of the decomposition temperature and ηtemp of 580 °C and 78%[36] respectively, whereas the values obtained in this study surpass those reported values. This is attributed to the low thermal conductivity of the PCB material. The thermal conductivity of FR-4, which is 0.2 W/m·K, is lower, compared to that of glass, the material with the lowest thermal conductivity (1.0 W/m·K) among those used in previous studies. The C* efficiency, η_{C^*}, was determined by comparing the theoretically calculated value of C* obtained by CEA with the experimentally calculated value obtained using Eq. (2). The experimentally calculated characteristic velocity, C*exp obtained using the measured chamber pressure and nozzle throat dimension yielded values of 772.59 m/s and 754.52 m/s for the horizontal and vertical thruster modules, respectively. The corresponding η_{C^*} values were 82.54% and 80.61% for each module type, respectively. The discrepancy between C^*_{exp} and the theoretical value can be attributed to the pressure drop caused by the excessive filling of the catalyst granules. Improvements can be achieved by optimizing the catalyst capacity, granule diameter, and chamber L/D ratio.

5.3 Performance test results: Thrust

To ascertain the performance and repeatability of the thrusters, a series of pulse-mode firing tests were conducted in three cycles for both the horizontal and vertical thruster modules (Fig. 8 and 9). A quantitative evaluation was performed considering the following parameters.

$$\eta_{\mathrm{F}} = F_{\mathrm{exp}}/F_{\mathrm{design}} \quad (5)$$

The thrust efficiency was determined using the following Eq. (5). Furthermore, the time required to ascend from 10% to 90% of the steady-state thrust is defined as the rising time, whereas the duration required to descend from 90% to 10% is denoted as the tail-off time. Nine thrust cycles were measured for each type of thruster module, and the coefficient of variance was employed to verify the repeatability of each parameter.

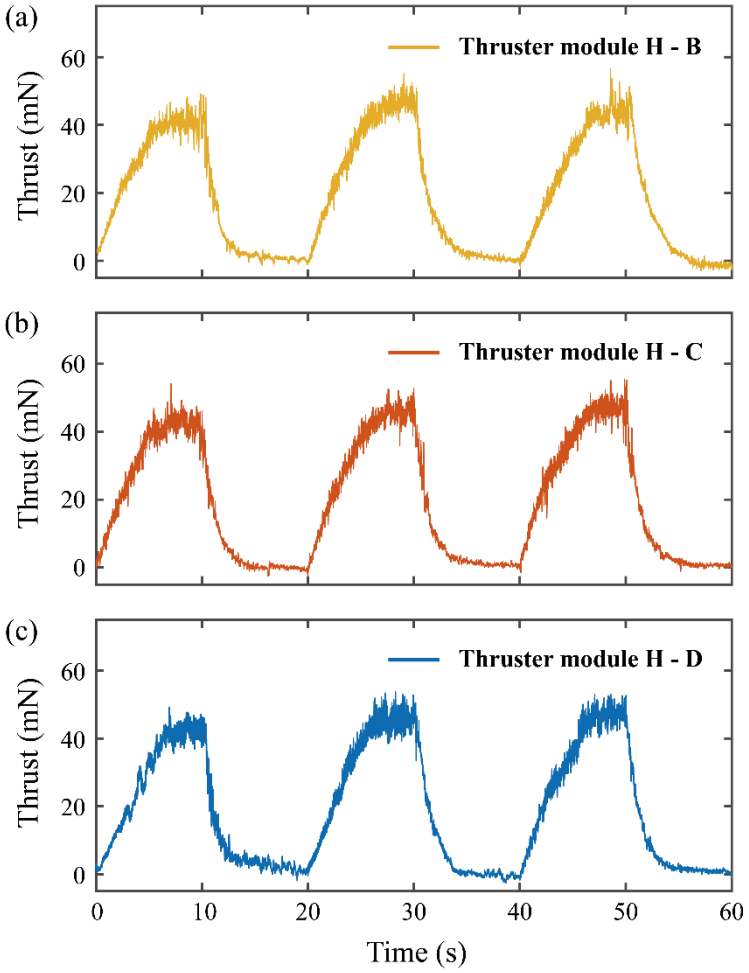

Fig. 8. Thrust measurement results of the horizontal thruster module (a) B, (b) C, and (c) D.

Table 3. Experimental results of three horizontal-type thruster modules.

	Rising time	Avg. thrust	Tail-off time
Thruster B	5.43 s	44.46 mN	3.37 s
Thruster C	4.97 s	45.06 mN	3.04 s
Thruster D	5.34 s	44.40 mN	2.78 s
Avg.	5.25 s	44.46 mN	3.06 s

In the horizontal-type thruster module, the average steady-state thrust was 44.64 mN, with a corresponding specific impulse of 78.32 s. The coefficient of variance for the thrust measurements in each cycle was 5.37%, confirming the consistent generation of thrust with a uniform magnitude. The calculated thrust efficiency η_F was 89.28%, based on the designed thrust value of 50 mN. The average rising and tail-off times were determined to be 5.25 s and 3.02 s, with the coefficient of variance measurements of 8.37% and 13.77%, respectively. Moreover, during the 30-second operational period, thruster B – D exhibited an ablation of the nozzle throat width by 17.75 μm, increasing from 608.62 μm to 626.37 μm, and the area expansion of 2.92% was accompanied. However, no ablation was observed in the height direction as the copper layer was positioned above and below.

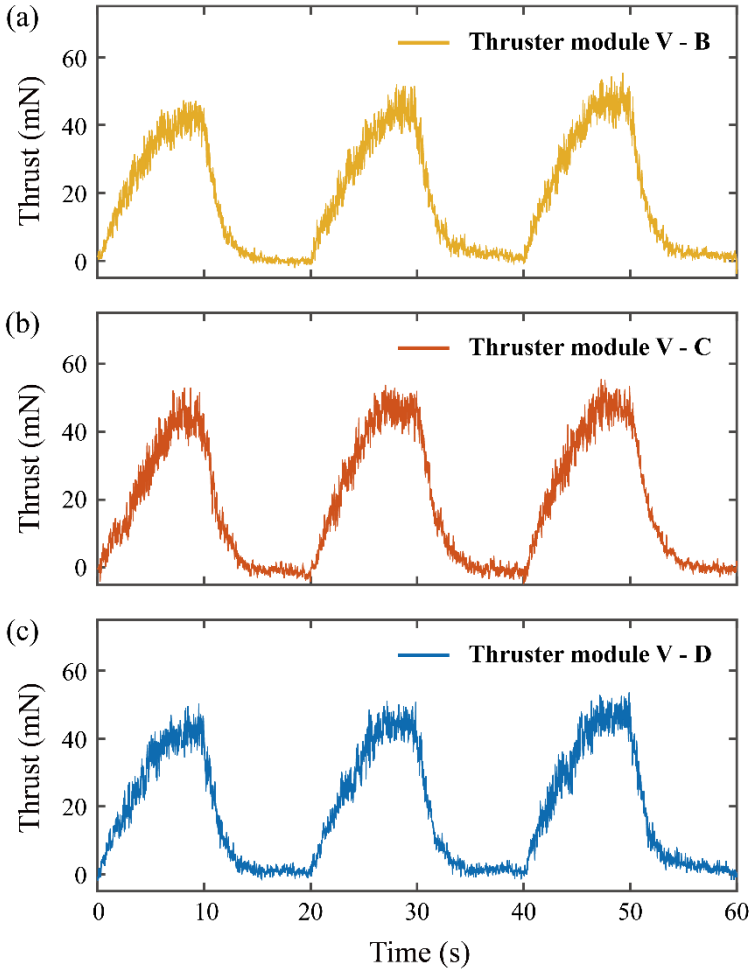

Fig. 9. Thrust measurement results of vertical thruster module (a) B, (b) C, and (c) D.

Table 4. Experimental results of three vertical-type thruster modules.

	Rising time	Avg. thrust	Tail-off time
Thruster B	4.73 s	44.28 mN	2.84 s
Thruster C	5.29 s	45.68 mN	2.95 s
Thruster D	4.89 s	44.28 mN	2.75 s
Avg.	4.97 s	44.87 mN	2.85 s

In the vertical-type thruster modules, the average steady-state thrust was 44.87 mN, with a coefficient of variance of 4.87%, indicating the repeated generation of thrust at a consistently uniform level. The calculated thruster efficiency η_F was 89.74%. Using this value, the specific impulse was driven for 78.72 s. The rising and tail-off times were 4.97 s and 2.85 s, respectively, with corresponding coefficients of variance of 9.12% and 7.88%. For thrusters B – D, the nozzle throat diameter expanded by 6.79 μm from 486.65 μm to 493.44 μm, and an area expansion of 2.81% was accompanied owing to ablation during the 30 s operational period. Overall, the observations indicated that both the horizontal and vertical thrusters exhibited similar thrust and propulsion characteristics. This finding suggests the feasibility of integrating thruster modules to construct customized propulsion systems with diverse performance capabilities.

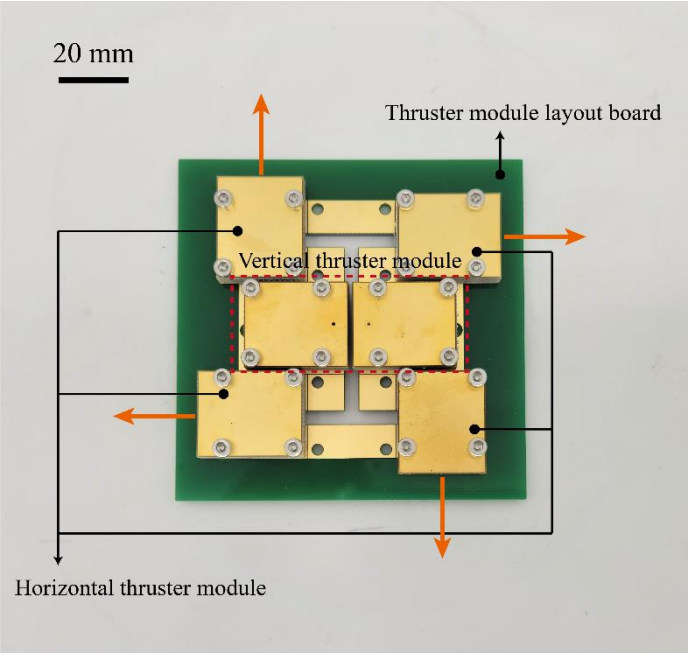

Fig. 10. Photo of assembled modular thrusters

Figure 10 illustrates the implementation of one of the applications proposed in Fig. 1(e). This design involves assembling four horizontal and two vertical thruster modules on a 10 × 10 cm thruster module layout board fabricated using a PCB. The assembly was performed by screwing M3 bolts after soldering. A thrust generation of 50 mN in the ±x and ±y directions and 100 mN in the +z direction was expected. Subsequent research efforts should be accompanied by the development of a propellant supply system that seamlessly integrates satellite hardware to enable the practical implementation of the aforementioned technology in nanosatellites. Furthermore, this development should be accompanied by comprehensive dynamic analysis and control performance testing conducted when the system is mounted on a satellite.

결 론

In this study, we present an engineering model of a 50 mN microthruster with both horizontal and vertical configurations fabricated using the lab-on-PCB technology. The main components-the injector, catalyst chamber, and nozzle-were constructed from five layers of a PCB and assembled using stencil printing and soldering, which are part of the PCB SMT processes. To assess the performance of the two thruster types and the viability of the lab-on-PCB technology, we employed an integrated pressure and temperature sensor within the thruster and measured the thrust using a load cell. During the propulsion test, the horizontal- and vertical-type thrusters demonstrated 84.44% and 85.31% thermal efficiency and 82.54% and 80.61% C^* efficiency, respectively, indicating that 90 wt.% hydrogen peroxide was sufficiently decomposed in each type of MnO_2/Al_2O_3-loaded PCB catalyst chamber, while also demonstrating effective heat retention. Furthermore, thrust efficiencies of 89.28% and 89.74% were calculated for horizontal- and vertical-type thrusters, respectively. Nozzle throat ablation was measured during a 30 s operating duration as 17.75 μm and 6.79 μm for the horizontal and vertical types, respectively. Notably, the performances of the two thruster variants were considerably similar. Overall, these outcomes suggest the promising potential of the lab-on-PCB technology for the repeatable fabrication of thruster modules. By addressing the limitations of existing MEMS-based thrusters, the lab-on-PCB technology offers the potential for upscaling and mass production through standardized processes while maintaining high durability and heat retention characteristics.

The modularized horizontal and vertical thrusters can be easily assembled on a thruster module layout

board, which is also composed of a PCB and subsequently integrated with the satellite body. Beyond the examples presented in this study, this approach enables the construction of propulsion systems optimized for specific satellite missions by customizing the type, number, and arrangement of thruster modules, similar to the assembly of Lego blocks. In future studies, we plan to evaluate the possibility of integration with satellites by considering the propellant supply module and testing the dynamic control performance through ground experiments. This methodology is anticipated to enhance the thruster supply capacity, addressing the growing market demand and diverse mission requirements of a constellation of nanosatellites.

참고문헌

[1] Addabbo, Pia, et al. "Contribution of Sentinel-2 data for applications in vegetation monitoring." Acta Imeko, vol 5, pp. 44-54, Jan 2016.

[2] Buzzi, Pau Garcia, et al. "Assessment of constellation designs for earth observation: Application to the TROPICS mission." Acta Astronautica, vol 161, pp. 166-182, Aug 2019.

[3] Marcuccio, Salvo, and Rafel Heitkoetter. "Environmental monitoring of the Amazon basin with a low cost small satellite constellation in equatorial LEO." 2018 IEEE International Conference on Environmental Engineering. IEEE, Jun 2018.

[4] Weiss, Werner W., et al. "BRITE-constellation: nanosatellites for precision photometry of bright stars." Publications of the Astronomical Society of the Pacific 126.940, Jun 2014.

[5] Curzi, Giacomo, Dario Modenini, and Paolo Tortora. "Large constellations of small satellites: A survey of near future challenges and missions." Aerospace 7.9, Sep 2020.

[6] Vuran, Mehmet C., et al. "Internet of underground things in precision agriculture: Architecture and technology aspects." Ad Hoc Networks 81, pp. 160-173, Dec 2018.

[7] Quinsac, Gary, et al. "Attitude control: A key factor during the design of low-thrust propulsion for CubeSats." Acta Astronautica, vol 176, pp. 40-51, Nov 2020.

[8] Lemmer, Kristina. "Propulsion for cubesats." Acta Astronautica, vol 134, pp. 231-243, May 2017.

[9] Silva, Marsil AC, et al. "A review of MEMS micropropulsion technologies for CubeSats and PocketQubes." Acta Astronautica, vol 143 pp. 234-243, Feb 2018.

[10] Gill, Eberhard, et al. "Formation flying within a constellation of nano-satellites: The QB50 mission." Acta Astronautica 82.1, pp. 10-117, Jan 2013.

[11] Muelhaupt, Theodore J., et al. "Space traffic management in the new space era." Journal of Space Safety Engineering, vol 6, pp. 80-87, Jun 2019.

[12] Hakima, Houman, and Michael CF Bazzocchi. "Low-thrust trajectory design for controlled deorbiting and reentry of space debris." 2021 IEEE Aerospace Conference (50100). IEEE, Jun 2021.

[13] Sutton, George P., and Oscar Biblarz. "Rocket propulsion elements." John Wiley & Sons, 2016.

[14] Lewis Jr, David H., et al. "Digital micropropulsion." Sensors and Actuators A: Physical 80.2, pp. 143-154, Mar 2000.

[15] Oh, Hyun-Ung, et al. "Verification of MEMS fabrication process for the application of MEMS solid propellant thruster arrays in space through launch and on-orbit environment tests." Acta Astronautica, vol 131, pp. 28-35, Mar 2000.

[16] Seo, Daeban, et al. "A MEMS glass membrane igniter for improved ignition delay and reproducibility." Sensors and Actuators A: Physical, vol 258, pp. 22-31, May 2017..

[17] London, A. P., et al. "Microfabrication of a high pressure bipropellant rocket engine." Sensors and Actuators A: Physical, vol 92, pp. 351-357, Aug 2001.

[18] Wu, Ming-Hsun, and Po-Shen Lin. "Design, fabrication and characterization of a low-temperature co-fired ceramic gaseous bi-propellant microthruster." Journal of Micromechanics and Microengineering 20.8, Jul 2010.

[19] Kuan, Chih-Kuang, Guan-Bang Chen, and Yei-Chin Chao. "Development and ground tests of a 100-millinewton hydrogen peroxide monopropellant microthruster." Journal of Propulsion and Power, vol 23, pp. 1313-1320, May 2007.

[20] Hitt, Darren L., Charles M. Zakrzwski, and Michael A. Thomas. "MEMS-based satellite micropropulsion via catalyzed hydrogen peroxide decomposition." Smart Materials and Structures, vol 10, Nov 2001.

[21] Cen, J. W., and J. L. Xu. "Performance evaluation and flow visualization of a MEMS based vaporizing liquid micro-thruster." Acta Astronautica, vol 67, pp. 468-482, Sep 2010.

[22] Miyakawa, Natsuki, et al. "MEMS-based microthruster with integrated platinum thin film resistance temperature detector (RTD), heater meander and thermal insulation for operation up to 1,000 C." Microsystem technologies, vol 18, pp, 1077-1087, Aug 2010.

[23] Kundu, Pijus, et al. "MnO2 Nanowire Embedded Hydrogen Peroxide Monopropellant MEMS Thruster." Journal of Microelectromechanical Systems, vol 22, pp. 406-417, Apr 2013.

[24] Khaji, Zahra, et al. "Alumina-based monopropellant microthruster with integrated heater, catalytic bed and temperature sensors." Journal of Physics: Conference Series. Vol. 757. No. 1. IOP Publishing, Aug 2016.

[25] Cheah, Kean How, and Kay-Soon Low. "Fabrication and performance evaluation of a high temperature co-fired ceramic vaporizing liquid microthruster." Journal of Micromechanics and Microengineering, vol 25, Dec 2014.

[26] Khaji, Zahra, et al. "Endurance and failure of an alumina-based monopropellant microthruster with integrated heater, catalytic bed and temperature sensors." Journal of Micromechanics and Microengineering, vol 27, Apr 2017.

[27] Markandan, Kalaimani, et al. "Fabrication and preliminary testing of hydroxylammonium nitrate (HAN)-based ceramic microthruster for potential application of nanosatellites in constellation formation flying." Microsystem Technologies, vol 25, pp. 4209-4217, May 2019.

[28] Huh, Jeongmoo, and Ki Sun Park. "Effect of Structural Materials on Monopropellant Thruster Propulsion Performance in Micro Scale." Aerospace, vol 10, Apr 2023.

[29] Plumlee, Donald, Judi Steciak, and Amy Moll. "Development and simulation of an embedded hydrogen peroxide catalyst chamber in low-temperature co-fired ceramics." International Journal of Applied Ceramic Technology, vol 4, pp. 406-414, Sep 2007.

[30] Wu, Ming-Hsun, and Richard A. Yetter. "A novel electrolytic ignition monopropellant microthruster based on low temperature co-fired ceramic tape technology." Lab on a Chip, vol 9, pp. 910-916, Dec 2008.

[31] Wu, Ming-Hsun, and Po-Shen Lin. "Design, fabrication and characterization of a low-temperature co-fired ceramic gaseous bi-propellant microthruster." Journal of Micromechanics and Microengineering, vol 20, Jul 2010.

[32] Lee, Jeongsub, et al. "Fabrication of catalyst-insertion-type microelectromechanical systems monopropellant thruster." Journal of Propulsion and Power, vol 28, pp. 396-404, Sep 2013.

[33] Huh, Jeongmoo, and Sejin Kwon. "Design, fabrication and thrust measurement of a micro liquid monopropellant thruster." Journal of Micromechanics and Microengineering, vol 24, Sep 2014.

[34] Huh, Jeongmoo, Daeban Seo, and Sejin Kwon. "Fabrication of a liquid monopropellant microthruster with built-in regenerative micro-cooling channels." Sensors and Actuators A: Physical, vol 263, pp. 332-340, Aug 2017.

[35] Kim, Ju Won, et al. "Room-temperature catalytically reactive ammonium dinitramide-H2O2 monopropellant for microsatellites." Advances in Space Research, vol 69, pp. 1631-1644, Feb 2022.

[36] Huh, Jeongmoo, et al. "Performance of MEMS-Based Monopropellant Microthruster With Insulating Effect." Journal of Microelectromechanical Systems, vol 31, pp. 612-624, May 2022.

[37] An, Sungyong. "Design and Microfabrication of Catalytic Reactor for a Micro Monopropellant Thruster." Master's thesis, KAIST, 2006.

[38] Köhler, Johan, et al. "A hybrid cold gas microthruster system for spacecraft." Sensors and Actuators A: Physical, vol 97, pp. 587-598, Apr 2002.

[39] Ranjan, R., et al. "Cold gas propulsion microthruster for feed gas utilization in micro satellites." Applied Energy, vol 220, pp. 921-933, Jun 2018.

[40] Rossi, C., et al. "Design, fabrication and modeling of solid propellant microrocket-application to micropropulsion." Sensors and Actuators A: Physical, vol 99, pp. 125-133, Apr 2002.

[41] Liu, Xuhui, et al. "Design, fabrication and test of a solid propellant microthruster array by conventional precision machining." Sensors and Actuators A: Physical, vol 236, pp. 214-227, Dec 2015.

[42] Moschou, Despina, and Angeliki Tserepi. "The lab-on-PCB approach: tackling the μTAS commercial upscaling bottleneck." Lab on a Chip, vol 17, pp.1388-1405, Mar 2017.

[43] Mueller, Juergen, et al. "An overview of MEMS-based micropropulsion development at JPL.", Apr 2001.

[44] Zhao, Wenhao, et al. "The review of Lab-on-PCB for biomedical application." Electrophoresis vol 41, pp. 1433-1445, Jan 2020.

[45] Liu, Robin Hui, et al. "Self-contained, fully integrated biochip for sample preparation, polymerase chain reaction amplification, and DNA microarray detection." Analytical chemistry, vol 76, pp. 1824-1831, Feb 2004.

[46] Boyd-Moss, Mitchell, et al. "Self-contained microfluidic systems: a review." Lab on a Chip, vol 16, pp. 3177-3192, Jul 2016.

[47] Salado, Guadalupe Flores. "Self-contained microfluidic platform for general purpose lab-on-chip using pcb-mems technology." Diss. Universidad de Sevilla, 2017.

[48] Chaalane, A., et al. "A MEMS-based solid propellant microthruster array for space and military applications." Journal of Physics: Conference Series. Vol. 660. No. 1. IOP Publishing, 2015.

[49] Simkin, Donald J. "Applications of Plastic Materials in Aerospace." No. 40. American Institute of Chemical Engineers, 1963.

[50] G. F. D'Alelio and John A. Parker, "Ablative plastics", Marcel Dekker, 1971.

[51] Rau, A. V., et al. "Resin transfer molding (RTM) with toughened cyanate ester resin systems." Polymer composites, vol 19, pp. 166-179, Apr 2004.

[52] Torre, L., J. M. Kenny, and A. M. Maffezzoli. "Degradation behaviour of a composite material for thermal protection systems Part I-Experimental characterization." Journal of materials science vol 33, pp. 3137-3143, Jun 1998.

[53] Lee, Doyun, Juwon Kim, and Sejin Kwon. "High performance microthruster with ammonium-dinitramide-based monopropellant." Sensors and Actuators A: Physical 283 (2018): 211-219.

[54] Lee, Jeongsub, and Sejin Kwon. "Evaluation of ethanol-blended hydrogen peroxide monopropellant on a 10 N class thruster." Journal of Propulsion and Power, vol 29, pp. 1164-1170, Sep 2013.

[55] Baek, Seungkwan, et al. "Development of high-performance green-monopropellant

thruster with hydrogen peroxide and ethanol." Journal of Propulsion and Power, vol 34, pp. 1256-1261, Jun 2018.

[56] Kang, Hongjae, et al. "A mixture of hydrogen peroxide and tetraglyme as a green energetic monopropellant." Combustion and Flame, vol 210, pp. 43-53, Dec 2019.

[57] Kim, Ju Won, et al. "Room-temperature catalytically reactive ammonium dinitramide-H2O2 monopropellant for microsatellites." Advances in Space Research, vol 69, pp. 1631-1644, Feb 2022.

[58] An, Sungyong, and Sejin Kwon. "Scaling and evaluation of Pt/Al2O3 catalytic reactor for hydrogen peroxide monopropellant thruster." Journal of Propulsion and Power, vol 25, pp. 1041-1045, Sep 2009.

[59] An, Sungyong, et al. "Comparison of catalyst support between monolith and pellet in hydrogen peroxide thrusters." Journal of Propulsion and Power, vol 26, pp. 439-445, May 2012.

[60] Heo, Seonuk, et al. "Effect of dual-catalytic bed using two different catalyst sizes for hydrogen peroxide thruster." Aerospace Science and Technology, vol 78, pp. 26-32, Jul 2018.

[61] Jo, Sungkwon. "Response characteristics of H2O2 monopropellant thrusters with MnO2-mixed PbO catalyst." Aerospace Science and Technology, vol 60, pp. 1-8, Jan 2017.

[62] Kim, Ju Won, et al. "Room-temperature catalytically reactive ammonium dinitramide-H2O2 monopropellant for microsatellites." Advances in Space Research, vol 69, pp. 1631-1644, Feb 2022.

[63] Huh, Jeongmoo, and Sejin Kwon. "Microcooling channel effect on a monopropellant microelectromechanical system thruster performance." Journal of Propulsion and Power, vol 33, pp. 1591-1595, May 2017.